

An optical laser device for mapping 3D geometry of underwater karst structures: first tests in the Ox Bel'Ha system, Yucatan, Mexico

Arnulf Schiller ⁽¹⁾, Philippe Renard ⁽²⁾

(1) Geological Survey of Austria, Department for Geophysics, Vienna.

Arnulf.Schiller@geologie.ac.at

(2) University of Neuchâtel, Centre of Hydrogeology and Geothermics, Neuchâtel.

Philippe.Renard@unine.ch

ABSTRACT

In the course of extended hydrological studies in the coastal Karst plain of Yucatan, near the town of Tulum amongst others, a novel laser scanning device was developed and applied for the acquisition of the 3d-geometry of ground water conduits. The method is derived from similar industrial systems and for the first time adapted to the specific measurement conditions in underwater cave systems. The device projects a laser line over the whole perimeter at a certain position. This line represents the intersection of a plane with the cave walls. The line is imaged with a wide angle camera system. Through proper design and calibration of the device it is possible to derive the true scale geometry of the perimeter via special image processing techniques. By acquiring regularly spaced images it is possible to reconstruct the true scale and 3 d-shape of a tunnel through the incorporation of location and attitude data. In a first test in the Ox Bel Ha under-water cave system, about 800 metres of tunnels have been scanned down to water depths of 20 metres. The raw data is further interpolated using the ODSIM-algorithm in order to delineate the 3D geometry of the cave system. The method provides easy, operable acquisition of the 3-D geometry of caves in clear water with superior resolution and speed and significantly facilitates the measurement in underwater tunnels as well as in dry tunnels. The data gathered represents crucial input to the study of the state, dynamics and genesis of the complex karst water regime.

Keywords: cave; geomorphology; geostatistics; Karst; 3D; laser scanner

Un dispositivo láser óptico para la cartografía 3D de la geometría de estructuras kársticas submarinas: primeros resultados en el sistema de Ox Bel'Ha, Yucatán, México.

RESUMEN

Durante el transcurso de intensivos estudios hidrológicos realizados en la llanura costera kárstica de Yucatán, cerca de la ciudad de Tulum entre otras, se desarrolló un novedoso dispositivo de escaneo láser, que se aplicó a la adquisición de la geometría 3D de conductos de agua subterránea. El método se deriva de sistemas industriales similares y que ha sido adaptado por primera vez a las condiciones de medición específicas de los sistemas de cuevas submarinas. El dispositivo proyecta una línea láser sobre todo el perímetro en una localización dada. Esta línea representa la intersección de un plano con las paredes de las cuevas. La línea es fotografiada con un sistema de cámara de gran angular. A través de un apropiado diseño y calibración del dispositivo es posible obtener la geometría verdadera del perímetro a través de técnicas especiales de procesamiento de imágenes. De este modo, adquiriendo regularmente imágenes a intervalos espaciados es posible reconstruir la escala verdadera y la forma 3D de un túnel con la incorporación de los datos de posición e inclinación. En una primera prueba en el sistema de la cueva submarina Ox Bel Ha, se escanearon

alrededor de 800 metros de túneles hasta profundidades, bajo el agua, de 20 metros. Los datos en bruto son interpolados utilizando el algoritmo de ODSIM para delinear la geometría 3D del sistema de cuevas. El método proporciona una adquisición sencilla y operativa de la geometría tridimensional de cuevas submarinas con aguas claras, con muy buenas resolución y velocidad lo que facilita la medición en conductos submarinos así como en túneles subaéreos. Los datos recogidos representan una información fundamental para el estudio del estado, dinámica y génesis del complejo régimen del agua kárstica.

Keywords: cueva, escaner laser, geomorfología, geoestadística, Karst, 3D.

VERSIÓN ABREVIADA EN CASTELLANO

Introducción

El complejo sistema de conductos kársticos de Ox Bel'Ha está situado en la costa sureste de la península de Yucatán, en el área de Tulum, México (Fig. 1). En el subsuelo, y debajo de la ciudad, toda el área se encuentra nervada por una vasta red de cuevas subacuáticas que se formaron en calizas con estratificación casi horizontal. El sistema de cuevas parece estar concentrado a profundidades que alcanzan hasta los 100 m. La capa más alta de agua dulce del acuífero kárstico representa prácticamente el único recurso de agua dulce en el área. Bajo la capa de agua dulce se encuentra el agua marina que penetra desde el mar y alcanza las regiones más profundas. El agua dulce está amenazada por un rápido desarrollo urbano y una gestión deficiente del agua residual. Además la situación es crítica porque las salidas de la red de conductos se localiza en la segunda mayor sistema de barrera arrecifal del mundo y la contaminación del agua subterránea también podría amenazar la reserva biológica UNESCO de Sian Ka'an, que se localiza a sólo unos pocos kilómetros al sur del área investigada. En este contexto, una gestión sostenible del agua así como una protección del arrecife y la bio-reserva requieren una mejor comprensión del recurso del agua y su potencial. Por este motivo, con las colaboraciones de NGO locales, diferentes universidades y el Servicio Geológico de Austria, se iniciaron en 2006 campañas de exploración subacuática que todavía continúan.

Contexto hidrogeológico y trabajos previos

El régimen de aguas subterráneas kársticas presenta un conocimiento limitado debido a su difícil accesibilidad. La red de conductos estudiada aquí es accesible a través de los cenotes, que representan partes colapsadas de conductos poco profundos, y a través de pozos. La dinámica del sistema está limitada principalmente a la capa de agua dulce, la haloclina o zona de mezcla y la parte superior del cuerpo de agua salada (Beddows, 2004, Gondwe, 2010a y 2010b). A través de varias campañas geofísicas se han adquirido diferentes tipos de datos, que comprenden la piezometría y el GPS diferencial para registrar las variaciones del nivel freático y la superficie haloclina; la distribución de la conductividad eléctrica en el subsuelo con métodos desde tierra y métodos desde aerotransportados para la cartografía de posibles conductos; diagráfias de sondeos, completado por análisis físicos y químicos del agua así como datos de topografías mediante la exploración de las cuevas por espeleobuceadores (Supper et al., 2009, 2010). Este extenso conjunto de datos proporcionan la información de entrada para un nuevo método de modelado pseudo-genético (Borghi et al., 2011, Vuilleumier et al 2013). En el modelo antiguo, los conductos eran representados como elementos 1D en una matriz 2D. Aquí, nos centramos en el desarrollo de herramientas para la adquisición de datos de la geometría 3D que se utilizará en el modelado del agua subterránea. Mientras las campañas electromagnéticas aerotransportadas en 2007 y 2008, más el procesado avanzado de datos desarrollados de 2012 hasta 2014, permitieron obtener una imagen global de toda la red de conductos ocultos (Schiller et al., 2010, 2012, 2013), el presente estudio se centra en una pequeña, pero representativa, parte de la red de conductos (Fig. 2). El objetivo es desarrollar una mejor comprensión de la génesis del sistema. Esto requiere un avanzado análisis químico y estructural, así como la adquisición de información detallada sobre la geometría 3D de conductos y datos de flujo en pasajes seleccionados. El escaneo 3D se logra con un dispositivo láser novedoso y metodología desarrollada especialmente para el trabajo en cuevas bajo el agua o subaéreas y que se presentan en este trabajo.

Método

El método consiste en un dispositivo para la toma de datos 3D de la forma de los conductos bajo el agua y el consiguiente procesado de imágenes incluyendo algoritmos avanzados de interpolación. El dispositivo

deriva de métodos industriales parecidos de escaneo láser aplicados en la medición de los tubos o para medición y control de calidad de procesos industriales (Kannala et al., 2008, Matsui et al., 2009). El diseño del dispositivo está pensado para que pueda ser usado por un espeleobuceador.

Dispositivo

El dispositivo (Figs. 3, 4) consiste en principio de una cámara UW y un láser UW que proyecta una línea láser sobre 360 grados, es decir, sobre el perímetro completo. Ambos componentes principales están conectados con una barra rígida de aluminio conservando una geometría especial de todo el sistema. Cuando este es nivelado bajo de agua del conducto y activado, la línea de láser se proyecta en la pared del túnel y genera una imagen con la cámara. Como ya se conocen los parámetros geométricos del sistema, se obtiene una función de mapeo que permite la transformación de la imagen de la línea láser con coordenadas locales en la imagen a coordenadas cartográficas reales. El resultado es una sección transversal a través del túnel. Las sucesivas capturas de secciones transversales pueden ser montadas en una representación 3D del túnel si se incorporaron en el proceso los datos sobre la posición y altitud del dispositivo.

Procesado

El primer paso de proceso consiste en digitalizar la línea láser que aparecen en la imagen. Esto se logra automáticamente mediante técnicas estándar de proceso de imágenes (Fisher y Naidu, 1991). El segundo paso consiste en transformar los datos con coordenadas de píxel a datos con coordenadas cartográficas reales mediante una función de mapeo (Fig. 5). El tercer paso es la compilación de sucesivas secciones transversales para formar un conducto 3D incorporar la información de altitud y posición (Figs. 8, 12). El último paso del proceso consiste en aplicar un método de interpolación geoestadística llamado ODSIM (Henrion et al, 2010).

Prueba en campo

Se diseñó un prototipo en la segunda mitad de 2012 y se preparó para una primera prueba de campo cerca de Tulum en marzo de 2013. Se han probado cinco líneas láser (cuatro azules y una roja), colocado en las cubiertas de una linterna subacuática. El sistema de toma de imágenes consistió en una cámara UW-DSLR con una lente ojo de pez de 4.5 mm. Durante las pruebas realizadas, para cada ubicación el dispositivo fue nivelado horizontalmente y ajustado paralelo a la línea. Antes de escanear las cuevas la calibración se ha realizado en aguas abiertas y se han tomado una serie de imágenes para calcular el tiempo de exposición óptima. En los consiguientes tests bajo el agua, se tomaron 270 secciones transversales capturadas en dos conductos durante tres inmersiones de aproximadamente 50 minutos cada una. La separación promedio es de aproximadamente de 3 m lo que da unos 800 metros de conducto escaneado.

Resultados y conclusiones

Las pruebas muestran que el dispositivo es ligero y práctico bajo el agua. El láser rojo fue rápidamente absorbido en la capa de agua dulce mientras el láser azul mostró solamente una débil absorción y cubrió bien el rango entero de diámetros hasta un máximo de aproximadamente 20 metros. En el agua salada el rango de láser azul, y también del rojo, fue también suficiente para las secciones grandes. En realidad, los láseres azules causaron sobreexposición, por lo que el tiempo de obturación tuvo que ser acortado. Después de la digitalización y el mapeo, los datos fueron visualizados como datos brutos en secciones transversales y fueron referidos a datos de la línea del conducto tomados en previas exploraciones subacuáticas (Figs. 6, 7). El método de interpolación-ODSIM produce una representación 3D como se ve en la figura 12.

Introduction and study area

The complex Ox Bel'Ha Karst conduit system is located on the southeast coast of the Yucatan peninsula in the region of the growing town of Tulum, Mexico (Fig. 1). In the subsurface, and below the city,

the whole area is criss-crossed by a vast network of underwater caves and conduits developed in nearly horizontal limestone layers which reach depths of several thousand of metres. The caves seem to be concentrated mainly to depths of 10 to 40 metres. However, in some places depths down to a maximum

of around 100 metres have been reached (Beddows 2004). The cave systems are world famous for their extension and their clear water. The upper most – or fresh water – layer of the karstic aquifer represents practically the only fresh water resource of the region (besides the higher lagoons which are located in a bio reserve and protected) since there is no surface discharge. The thickness of the fresh water layer develops from zero at the coast to some 15 to 30 meters with distances from the coast reaching 15 to 25 kilometres. Below the fresh water layer there is salt water intruding from the sea and reaching the deeper regions. The fresh water is endangered by rapid urban development and insufficient plans for a sustainable water management. Furthermore, the situation is critical because submarine outlets of the conduit network are located at the coast right between the town of Tulum and an urban development area and the second largest barrier reef system of the world and can deliver pollutants through the ground water to the reef. Ground water contamination is also potentially endangering the nearby Sian Ka'an UNESCO world heritage biological reserve, located to south of the survey area and famous for its species in mangroves and lagoons. In this context, careful water management planning as well as the protection of the reef and the bio-reserve requires a better understanding of the karst water regime and its potential (initial, regional scale approaches are described in Gondwe, 2010a and 2010b, Bauer-Gottwein, 2011). For this reason, different collaborations of local

NGO, exploration divers, various universities and the Geological Survey of Austria were initiated in 2006 and are still in progress.

Underground karst water regimes are little understood due to their difficult accessibility. The conduit network studied here is accessible through 'Cenotes' which represent collapsed parts of shallow tunnels with open water, and through wells or bore holes (Fig. 2). The dynamics of the system is mainly constraint to the freshwater layer, the halocline or mixing zone and the uppermost part of the salt water body (Beddows 2004). In the mixing zone of the halocline the potential for lime stone rock solution increases (Fisher and Naidu, 1991). Therefore, level changes (long term geological changes due to ice ages as well as seasonal one down to very short term variations due to tides) of the halocline govern the depth range and velocity of cave development. Of course, the cave- or conduit system in the depth range of the fresh water layer is most relevant since it provides the transportation network for replenishment – and also for spreading contamination.

To develop a deeper understanding of the structure and dynamics of the systems in the course of several geophysical campaigns different data has been acquired comprising piezometry and differential GPS for assessing variations in the water table and the halocline surface; electrical conductivity distribution in the subsurface with ground and airborne methods for mapping the distribution of potential conduits; ground penetration radar, borehole

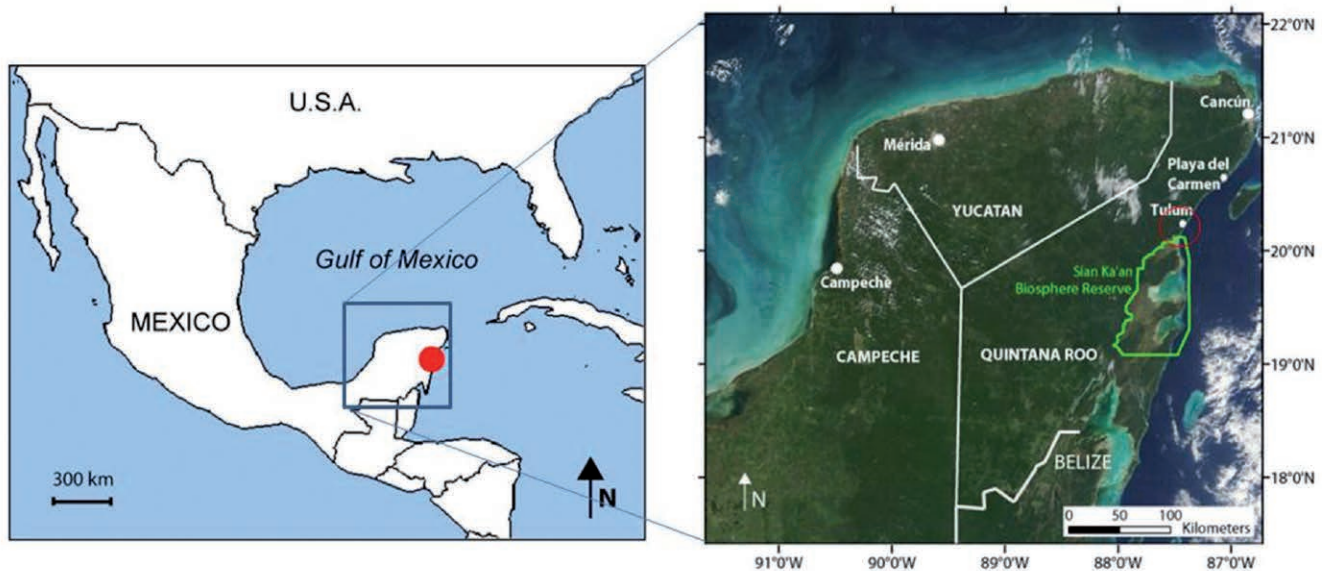


Figure 1: Location of the survey area.

Figura 1. Localización del área de estudio.

geophysics for punctual and detailed acquisition of electrical conductivity, rock density / porosity and stratification of the lime stones, completed by chemical and physical water analysis as well as cave survey data from exploration divers (Supper *et al.*, 2010). This extensive data set provided the input for a pseudo-genetic modelling (Borghetti *et al.*, 2011, Vuilleumier *et al.*, 2013) which described the karstic network as 1D elements embedded in a 2D matrix.

Objectives

While the airborne electromagnetic surveys of 2007 and 2008, plus advanced data processing methods developed in 2012 to 2014, yielded remarkable results and an exceptional clear over all image of the hidden conduit network (Schiller *et al.*, 2010, 2012, 2013), this study is focused on a small but representative part of the network (Fig. 2). The goal of the study is to gain a deeper understanding of the genesis of the system and derive realistic parameters for the hydrological modelling approach. This requires advanced chemical and statistical structure analysis, as well as the acquisition of detailed information on the 3D-conduit geometry and water flow data in the selected tunnels.

This is the context in which the described development contributes. The aim of this study was the design of a device with which important 3D-geometric data could quickly be acquired with superior resolution under the very specific measurement conditions in underwater caves.

Principle of the method

The measurement principle is derived from similar laser scanning methods as applied for measuring task

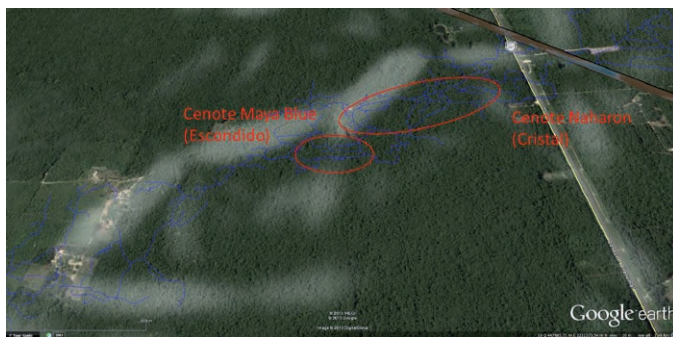


Figure 2: Part of the cave system chosen for the field tests.
Figura 2. Partes del sistema de cuevas elegidas para pruebas de campo.

in industrial processes (Kannala *et al.*, 2008, Matsui *et al.*, 2009), adapted to the special measurement conditions in under water caves. An essential pre-condition for this optical method is clear water which is uniquely fulfilled in the case of the under-water karst tunnels and caverns around Tulum, where visibilities reaching 100 up to 250 metres are reported in the local exploration divers' community. The method developed provides the imaging hardware for capturing the shape of the perimeter of the tunnels as well data processing algorithms comprising special image processing and novel interpolation algorithms preserving statistical characteristics of measured data in the interpolated data.

Design principle

The device (Figs. 3, 11) consists in principle of a camera and a laser head projecting a laser line over 360 degrees, i.e., over the whole perimeter of a tunnel. This laser line can be thought of as consisting of a large number of laser points, each one projected by a single laser ray. All the rays are gathered in a plane, designated as a laser plane. Both the main components of the device (protected by a water-proof casing) are connected through a rigid bar made of aluminium preserving a specially intended geometry of the system.

The basic principle is triangulation. The system camera – an optical axis of imaging system – laser ray - point of the projected laser line on the tunnel wall forms a rectangular triangle with 90° between

Principle of a mobile measurement set up for cross section capturing of under water caves

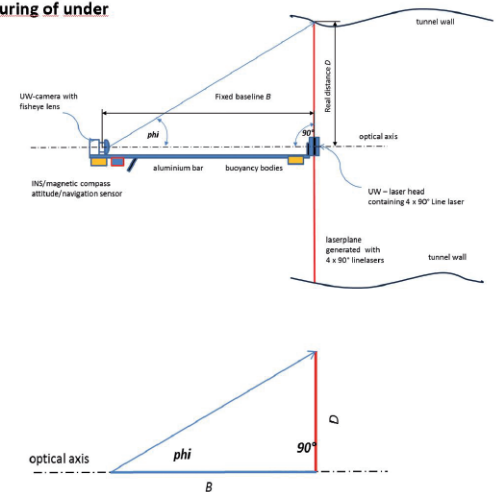


Figure 3: Basic principle of the scanning method.
Figura 3. Principio básico del método de escaneo.

the optical axis and some laser rays as shown in Figure 3. The separation between the camera and the laser plane is fixed by design and represents the base line B . The crossing point of the optical axis through the laser plane is here defined as the centre O of the laser-plane coordinate system which is two dimensional with z upwards and x to the right.

An observer at the position of the camera and looking at a specific point of the laser line on the tunnel wall would recognize a certain angle ϕ between the optical axis and the line of sight to the specific laser point on the tunnel wall. Assuming the length of the base line is known it is possible to simply calculate the distance D of the specific point from the centre of the laser plane through

$$D = B \cdot \tan(\phi) \quad (1)$$

The question is how to measure ϕ . This is done by the imaging system since every angle in real world system maps to a certain distance in pixel coordinates (or pixel distance) p as

$$p = \text{imap}(\phi) \quad (2)$$

onto the image. This pure geometrical imaging function imap is specified and documented for numerous cameras/optics configurations. Consequently, the inverse mapping function gives the angle

$$\phi = \text{imap}^{-1}(p) \quad (3)$$

from the pixel distance between the optical axis (usually the centre of the image) and the specific laser point on the imaged tunnel wall. Since the optical distortion of the imaging system is axial-symmetric referred to the optical axis, the mapping function is axial-symmetric as well. This means that the only important parameter for obtaining the real distance D of the laser point from the laser plane centre is the pixel distance p .

$$D = B \cdot \tan(\text{imap}^{-1}(p)) \quad (4)$$

This calculation can be done for every point along the imaged laser line. The real distance can then be

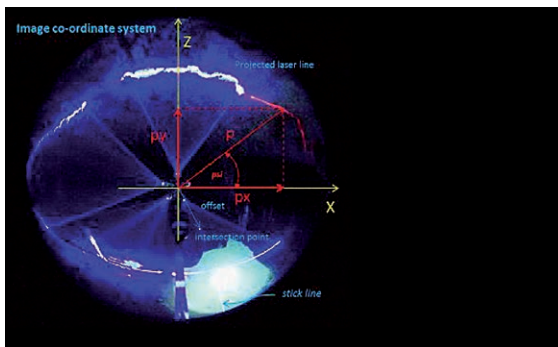


Figure 4: Laser plane co-ordinates in an image system.
Figura 4. Coordenadas del laser avión en el sistema de imagen.

split into z and x components in the laser plane system, taking into account the second important angle ψ between z axis and laser ray from the centre of the laser plane to a specific point of the laser line (Fig. 4). This angle is mapped directly to the image without distortion if axial symmetry assumed (since the optical axis of the system is perpendicular to the laser plane by design). Herewith the problem is comfortably solved in the ideal case.

Calibration

The real case that emerges is more complex. Geometric errors in the instrument's design introduce non-axial symmetric behaviour of the mapping function. The effective length of the base line depends on the lens system. The angular distortion is additionally affected by light refraction at the water-dome-air interfaces when light passes from the water into the water-proof casing. All these combined effects can be considered by a simple calibration procedure in which a scale bar or tape is placed onto the laser plane and imaged. The image of this scale under measurement conditions, i.e. in the water, gives the over-all mapping function directly by counting the pixel distance to a certain cm-mark of the imaged scale (Fig. 5). Equations (1) to (4) plus effects not considered herein can then substituted by a direct relation between real distance D and imaged distance p

$$D = \text{calmap}(p) \quad (5)$$

The computational realization of this mapping is a simple look-up table operation.

Positioning

In the presented test survey, the cross sections positions are related to the 'stick line'. The stick line represents a tunnel's geometry as a series of connected straight lines, similar to sticks (Fig. 6). In reality it is a cord, attached onto rocks in the cave and other suitable features on the tunnel wall. So the stick line is not equivalent with the (mean) tunnel axis. The stick line is measured by exploration divers with a compass, inclinometer and scale tape in dead reckoning technique. The normal offset of a laser scanned cross-section to the stick line is visually well defined by the intersection of the laser plane with the cord as indicated by a bright dot where the line laser illuminates the cord. After mapping this gives the in-plane offset of the laser plane coordinate system relative to the stick line if the instrument is horizontally levelled and aligned parallel to the stick line. The position

Calibration - mapping function

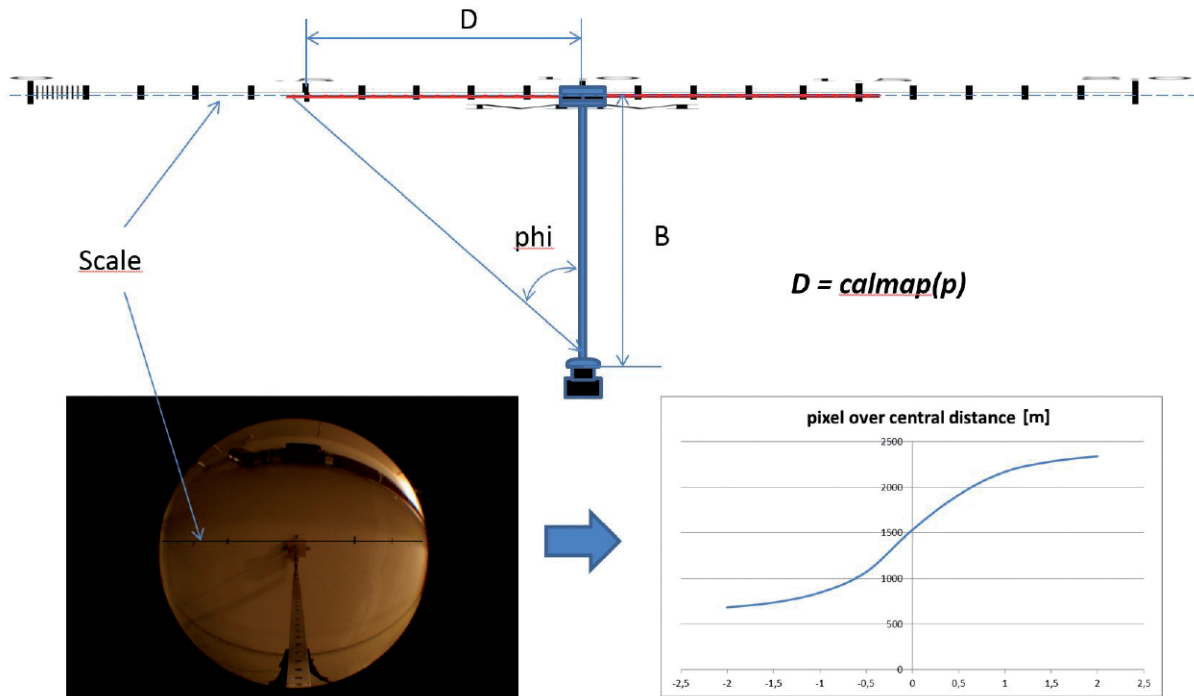


Figure 5: Principle of calibration procedure. Bottom right paragraph: calibration mapping function.

Figura 5. Principio del proceso de calibración. Parte inferior derecha del párrafo: mapeo de la función de calibración.

along the line is defined by equally spaced intervals of approximately three metres. The diver tries to keep the spacing constant. Additionally, along each straight leg of the stick line the spacing is averaged.

Processing

The processing here is explained for one image (shot). It is exactly the same for all the shots acquired during a tunnel-scan survey, which can be in the order of several hundreds during one dive.

The first processing step is digitizing the image data. This can happen automatically by standard image processing techniques (Fisher and Naidu, 1991). However, manual editing gives the opportunity of interpreting gaps in the laser line (shadows or side tunnel or line out of measurement range (Fig. 7). The second step is transforming the data from pixel coordinates to real-world coordinates by means of the mapping function (5) (Fig. 5). In principle this is done with a look-up table as soon as the mapping function is known from calibration. The result of digitizing and mapping is a set of local laser plane

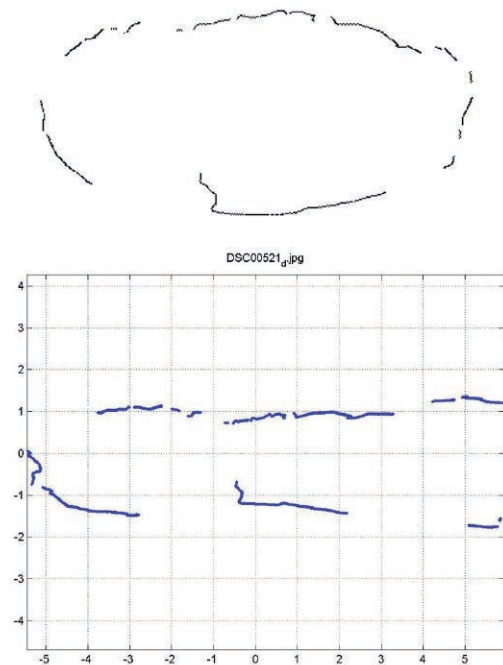


Figure 6: Top: digitized cross section. Bottom: mapped cross section.
Figura 6. Arriba: digitalizado de la sección transversal. Parte inferior: trazado transversal.

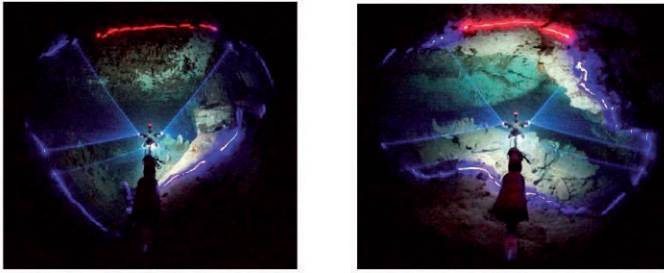


Figure 7: Top: two cross section shots. Bottom: mapped cross sections connected to stick line.

Figura 7. Arriba: Dos disparos de sección transversal. Abajo: secciones transversales mapeadas conectadas para pegar la en línea.

coordinates of a few thousand points along the laser line projected, i.e., one cross section through the tunnel. The third processing step is the compilation of successive cross sections of successive shots to the 3-d representation of the scanned tunnel by incorporating attitude and position information (Figs. 6, 7, 8).

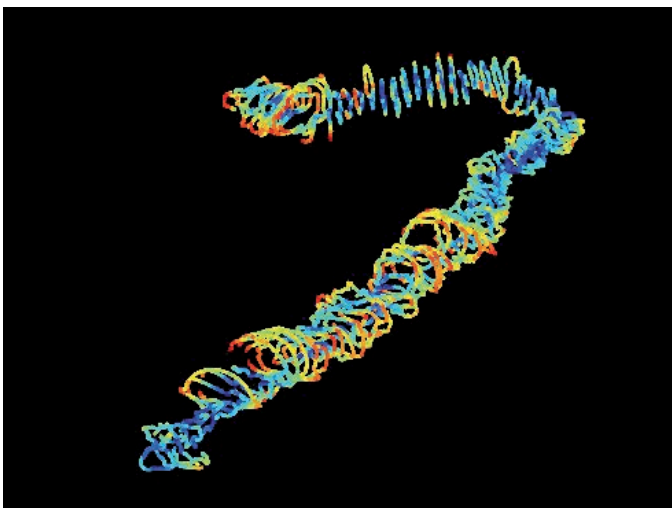


Figure 9: Cenote Maya Blue – The points from the 77 shots are coloured with the distance to the centreline.

Figura 9. Cenote Maya Blue – Los puntos de los 77 disparos están coloreados con la distancia hasta la línea central.

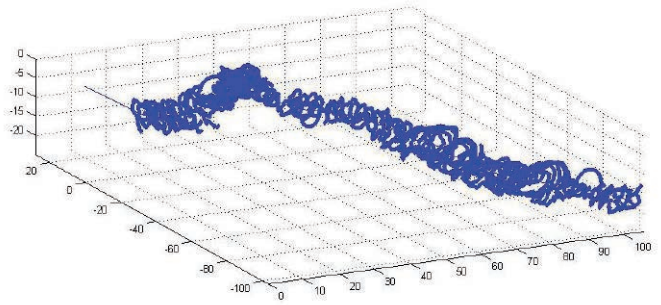


Figure 8: Maya Blue Cenote– A- tunnel scanned with 77 shots.
Figura 8. Cenote Maya Blue - A – túnel escaneado con 77 disparos.

The final processing step is based on a modified version of the statistical interpolation method named ODSIM (Henrion *et al.*, 2010). The general idea of ODSIM is to use one random field and one distance field and to declare that the points such that the distance is below the threshold belong to the karstic system. We will not repeat here all the methodology described in Henrion *et al.* (2010) but will only summarize the main steps. All the methodology was applied using Matlab and Sgems (Remy *et al.*, 2011) for the geostatistical calculations. The first step of the method is to define a volume around the conduit and to discretize it with a regular grid. Only the points in the surroundings of the observations are considered in the next steps. This allows minimizing computing cost and increasing resolution. First, the minimum distance $d(x,y,z)$ between any point in the domain and the centre line is computed for all the nodes and stored in the 3D grid. The centre line is the line that

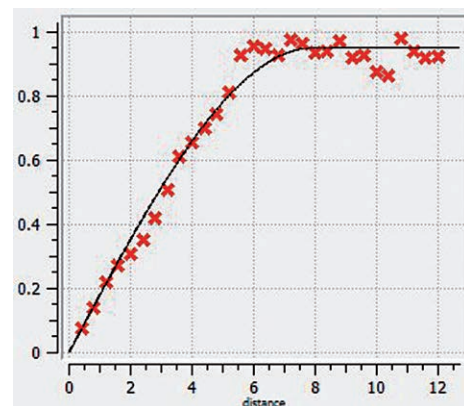


Figure 10: Variogram of distance to the centre line (after normal score transform) as observed in the data points.

Figura 10. Variograma de la distancia hasta la línea central (después de transformar la puntuación normal) como se observa en los puntos de datos.

goes through the centre of each section. Once this step is done, we also compute the distance to the centre lines for all the points that were obtained with the scanning device (Fig. 9).

This set of points with measured distances is analyzed and their univariate and spatial statistics are studied (histogram, variogram). In our example, the distances have a slightly skewed distribution with a median value of 2.6 m and are comprised between 0.3 and 7 m to the centre line. Consequently, we only consider for this example, the area having a distance to the centre line below 8 m to make the computations. The distances at the data points are then transformed into a normal distribution using the normal score transform algorithm. Figure 10 shows the experimental and model variograms of the corresponding normalized data. They show a nice fit with a spherical model of range 8.4 m and a sill of 0.95.

The next step is to simulate in 3D a stochastic distance field using conditional sequential Gaussian simulations (SGS) with the parameters inferred from the previous step. The SGS is back transformed. It results in a 3D field defined everywhere in the region of interest where a simulated distance to the centre line is available. Let us denote it as $s(x,y,z)$. Because of the statistical nature of the method, several simulations can be obtained. They are all conditional to the observations, meaning that the value of $s(x,y,z)$ is exactly the one that has been measured at the data points but may be different from one realization to another in the other points. Finally, the two fields are compared, and the rule is that a grid cell is declared to belong to the karstic cavity if $d(x,y,z) < s(x,y,z)$. As discussed in Henrion *et al.* (2010), this method may generate artefacts, i.e., zones in the cavities that are not considered to belong to the cavity or vice-versa. To reduce those artefacts, we modified the algorithm of Henrion *et al.* (2010), by generating a locally varying mean for the sequential Gaussian simulations. This was taken as $m(x,y,z) = 5 \exp(-0.5 (d(x,y,z)/2)^2)$. Doing so, the simulated values for $s(x,y,z)$ are more likely to be high close to the centerline and to decrease further away. One resulting simulation is shown in Figure 12.

Sources for possible errors

The method is developed and designed to achieve the most comfortable acquisition of high resolution cross section geometry data while minimizing errors introduced by measurement and processing, nevertheless different sources for potential have to be considered (Table 1).

Calibration error

The calibration procedure considers all the geometric and refractive distortion of the system, assuming the laser plane is perfectly flat and the optical axis of the imaging system is normal to the laser plane. In this case the mapping function is axial symmetric and can be retrieved by imaging a scale bar or tape positioned in the laser plane crossing through the centre. If the optical axis of the imaging system is not perfectly normal to the laser plane, the mapping function becomes non-axial symmetric. Spread into two dimensions the mapping function transforms from circular to elliptic. Determination of this 2 dimensional elliptic mapping function would require far more elaborate 2d-calibration with a 2d-grid instead of a linear scale. However, non-axial symmetric errors can be limited to centimetre accuracy by exactly aligning the optical axis of the lens/dome system perpendicular to the laser plane. The flatness of the laser plane is achievable by adjusting each laser and checking the coincidence of the individual lines optically and through rotation of the laser head around the optical axis of the system.

Positioning error

The position of a cross section is combined from the position of the cross section relative to the stick line and the position of the intersecting point on the stick line. The relative position and orientation of the cross-section is defined by horizontal levelling of the device and parallel aligning the horizontal components of stick line and optical axis of the system. While horizontal levelling is well controllable via sensors, the parallel aligning depends on the quality of the diver's estimation, so angular errors of a few degrees are possible. The error-contribution of in-plane offset as indicated by the bright point, where the laser line highlights the stick line is in sub-centimetre range.

The stick line is measured by exploration divers with a compass, inclinometer and scale tape in a dead reckoning technique. Where possible, the measurement error introduced by imperfect heading, inclination and scale reading is corrected by connecting the measurement to fixed points, i.e., exits, where possible, or by forward and backward measurement for defining a loop error. The error can increase into the range of metres if the path is several hundreds of metres away from the next fixed point.

Error source	Magnitude
Calibration	1mm to 5 cm at 15 metres centre distance
Digitizing	1mm to 5 cm at 15 metres centre distance
Positioning	decimetres to metres, depending on the complexity of the system

Table 1: Magnitude of errors.

Tabla 1. Magnitud de los errores.

Digitizing error

A different type of error is introduced by imperfect digitizing, especially at the margins of the image i.e., at large values of *phi*, significant compressing of imaged distances takes place due to the specific behaviour of the mapping function. So, even small errors in the digitized perimeter can map to significant errors in the mapped cross section. A practical consequence of this fact is setting an upper limit for the angle *phi* and skipping points too close to the margins of the image. Careful editing is required, especially when approaching this limit.

Interpolation Error

The magnitude of the uncertainty on the position of the cave in between the measurements can be estimated by using an ensemble of simulations. Then, by making statistics over the ensemble it is possible to get an envelope of the possible position of the cavity. This rather straight forward approach in geostatistics has not yet been applied here but should not pose any problem.

Field test

A prototype was designed in the second half of 2012 and prepared for a first field test in Tulum in March 2013. The tunnels scanned are located in the Ox Bel Ha system and accessible through the Maya Blue Cenote (Fig. 2). Five line lasers (four blue and one red) have been chosen and installed with batteries and tilt switch into underwater lamp casings each. The casings were mounted on a plate through joints and adjustable in 3 degrees of freedom in angle. The laser plane was well adjustable. The imaging system consists of a DSLR camera with 4.5 mm circular fish-eye lens protected by an underwater casing. For adjusting the balance of the device under water,

Maya Blue Cenote (hidden)			Diver:
A-tunnel			
	- first test:	125 shots	Robbie Schmittner
	- second test:	77 shots	Richie Schmittner
Dead zone	- third test:	71 shots	Richie Schmittner

Table 2. Field test scans.

Tabla 2. Pruebas de escaneos sobre el terreno.

two aluminium bottles mounted onto the bar were filled with a proper amount of water. The lasers were switched off with tilt switches by rotating the device and automatically activated when the device was levelled. For levelling acceleration sensors integrated in the camera and tilt indicators on the camera display, as well as a bubble level mounted onto the bar, have been used. At each shot the device was levelled horizontally and adjusted parallel to the line. The position along the line was defined by approximately equal separation along a straight leg of the line. Prior to the first cave scan, calibration tests have been conducted in open water and image series have been taken to find the optimum exposure time. In course of the following under water tests about 270 cross sections have been captured in two tunnels during three dives of approximately 50 minutes each. With an average separation of approximately 3 metres, this gives some 800 metres of scanned tunnel (Table 2).

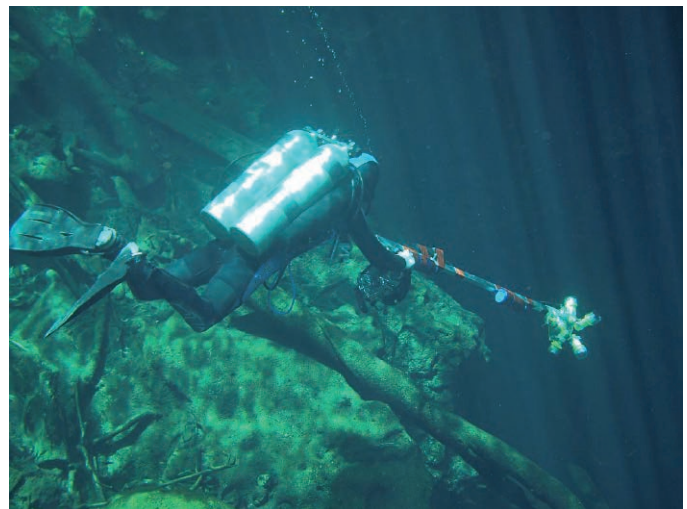


Figure 11: Richie Schmittner starting the second dive in A-tunnel.

Figura 11. Richie Schmitter iniciando la segunda inmersión en A-tunnel.

Results

The tests showed that the device is light and easy to operate under water. An additional front light is of advantage for the orientation of the diver as well as for interpretation purposes during later image processing, e.g. distinguishing between laser line gaps caused by side tunnels or shadows caused by rocks. A typical raw image is shown in Figure 13. The tilt switches worked well. The red laser was quickly absorbed in the fresh water layer while the blue laser showed non-critical absorption and covered the whole diameter range up to 20 metres well. The dome of the imaging system restricted the range due to refraction. In salt water the range of blue as well as red laser was also sufficient for the bigger cross sections. In fact, the blue lasers caused overexposure so the shutter time had to be decreased. The touch point of the laser plane with the stick line for off set correction is clearly visible. Due to refraction gaps the stick line was not lit in every shot. After digitizing and mapping the data was visualized as raw data in single cross sections and combined with stick line data from under water cave surveys (Figs. 7, 8). The Odsim-interpolation method leads to 3D models such as the one seen in Figure 12. This preliminary result demonstrates that the method can be used to define the geometry of the karstic system.

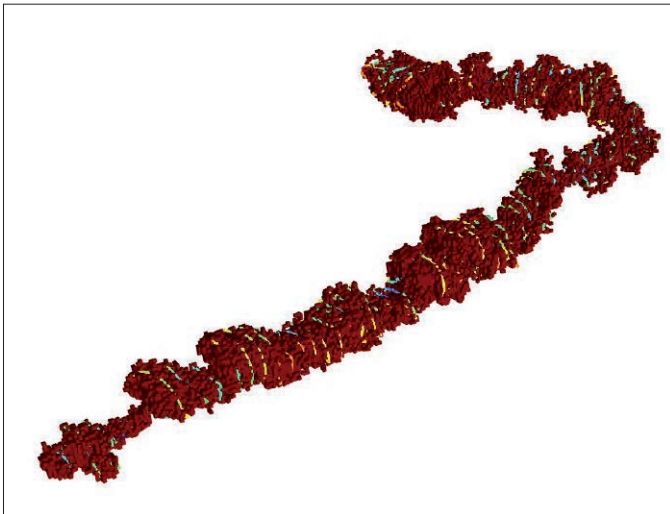


Figure 12: Resulting volume obtained by the Odsim interpolation method superposed with the data points from the section coloured with distance to the centreline.

Figura 12. Volumen resultante obtenido por el método de interpolación Odsim superpuesto con los puntos de datos de la sección coloreada con la distancia hasta la línea central.

Discussion and the next steps

The first prototype worked well and delivered the required geometry data. For the next survey, which is in preparation, specific advancements are at the development state and will be tested. The main improvements are a new laser head for achieving a laser plane without gaps with fewer lasers and the integration of three-axis translation acceleration, angular acceleration and magnetic heading sensors, as well as a pressure sensor used for inertial navigation / water depth measurement. Post-processing of this data will enable a better estimation of the path and attitude of the system. Correction will be introduced by resting the instrument on the ground (acceleration $a_i=0$, speed $v_i=0$) in proper time intervals and fitting the z-coordinate to the measured water depth. The tilt and heading data of the sensor is also used to process cross-sections captured with arbitrary orientation of the device. This is of special advantage in small tunnels with high inclination where the instrument can hardly be levelled horizontally. The lasers are activated via cable and flash synchronization signal for only 0.5 seconds which helps to save power. Future advancements will concern a full 180° dome to avoid additional refraction. This dome has to be specially manufactured. The issue of an independent under water positioning is still acute. An interesting approach is a VLF radio transceiver system which may be tested in the course of the next field campaign. Advanced processing of the IMU-sensor data will also permit better positioning results.

With this handy device important geometric parameters can be quickly captured both under water and in dry caves. The method gives several thousand perimeter points with one shot, i.e., in 0.2 seconds – so the acquisition speed, resolution and information density is superior to other methods. The data provides a generous basis for hi-resolution analysis for quantities such as cross section area shape and roughness parameters which may be utilized in further analysis, simulation or modelling.

The interpolation results presented above are still preliminary and a number of further tests must be conducted to validate the methodology. This work is planned to be pursued in the near future.

Acknowledgments

We are very grateful for the great support given by the “Amigos de Sian Ka’an”, Robert and Richard Schmittner (Xibalba Diving Center), Bill Phillips (Speleotech), Simon Richards, as well as the Austrian



Figure 13: Perimeter scan in a hall known as the 'cathedral' in the A-tunnel section below the halocline.

Figura 13. *Perímetro de exploración en una sala denominada 'catedral' en la sección A-tunnel por debajo de la haloclina.*

Science Fund and the Swiss National Science Foundation who financed this joint project XIBALBA (I994-N29), and the Geological Survey of Austria.

References

- Back, W., Hanshaw, B.B., Thomas, E., Pyle, L., Plummer, N., and Weidie, A.E. 1979. Geochemical significance of groundwater discharge and carbonate solution to the formation of Caleta Xel Ha, Quintana Roo, Mexico. *Water Resources Research*, 15(6), 1521-1535.
- Bauer-Gottwein, P., Gondwe, B. R. N., Charvet, G., Marín, L. E., Rebolledo-Vieyra, M., Merediz-Alonso, G. 2011. Review: The Yucatán Peninsula karst aquifer, Mexico. *Hydrogeology Journal*, 19(3), 507-524.
- Beddows, P.A. 2004. Groundwater hydrology of a coastal conduit carbonate aquifer: Carribean coast of the Yucatán Peninsula, México. PhD Thesis, University of Bristol, Bristol, 303 pp.
- Borghi, A., Renard, P., Jenni, S. 2012. A pseudo-genetic stochastic model to generate karstic networks. *Journal of Hydrology*, 414-415, 516-529.
- Fisher, R.B., and Naidu, D.K. 1991. A comparison of algorithms for subpixel peak detection. *Proceedings of the 1991 British Machine Vision Association Conference (BMVAC 1991)*, pp.217-225.
- Gondwe, B. R. N., 2010. Exploration, modelling and management of groundwater-dependent ecosystems in karst – the Sian Ka'an case study, Yucatan, Mexico. PhD Thesis, Technical University of Denmark, Kongens Lyngby, 86 pp.
- Gondwe, B. R. N., Lerer, S. M., Stisen, S., Marin, L., Rebolledo-Vieyra, M., Merediz-Alonso, G., Bauer-Gottwein, P. 2010. Hydrogeology of the south-eastern Yucatan Peninsula: New insights from water level measurements, geochemistry, geophysics and remote sensing. *Journal of Hydrology*, 389(1-2), 1-17.
- Henrion, V., Caumon, G., Cherpeau, N., 2010. ODSIM: An Object-Distance Simulation Method for Conditioning Complex Natural Structures. *Mathematical Geosciences*, 42(8): 911-924
- Kannala, J., Brandt, S.S., and Heikkilä, J. 2008. Measuring and modelling sewer pipes from video. *Machine Vision and Applications*, 19(2), 73-83.
- Matsui, K., Yamashita, A., and Kaneko, T. 2009. 3-D shape reconstruction of pipe with omni-directional Laser and omni-directional camera. *Proceedings of the 3rd International Conference of Asian Society for Precision Engineering and Nanotechnology (ASPEN2009)*, 1A2-15, pp.1-5.
- Remy, N., Boucher, A., Wu, J., 2011, *Applied Geostatistics with SGeMS: A User's Guide*. Cambridge University Press, Cambridge, 286 pp.
- Schiller, A., Klune, K., and Schattauer, I. 2010. Advanced AEM by comprehensive analysis and modelling of system drift. *EGU General Assembly 2010, Geophysical Research Abstracts*, 12 EGU2010-11995-1.
- Schiller, A., Supper, R., Vuilleumier, C., Ottowitz, D., Ahl, A., and Motschka, K. 2012. Airborne and ground geophysics for modelling a karstic conduit system: New results from the 2007-2011 campaigns in Tulum. *Near Surface Geoscience 2012, Remote Sensing Workshop, Proceedings of the 18th European Meeting of Environmental and Engineering Geophysics*, Paris.
- Schiller, A., Supper, R., Merediz Alonso, G., Ottowitz, D., Vuilleumier, C., Motschka, K. 2013. Aero-electromagnetic mapping of the hidden ground water conduit systems beneath the Tulum Karst plains. *IAGA, 12th scientific assembly, Merida, August 26-31, 2013, abstracts 1.3-7, abstract volume p. 102.*
- Supper, R., Motschka, K., Ahl, A., Ottowitz, D., Bauer, P., Gondwe, B., Merediz Alonso, G., Römer, A., Kinzelbach, W. 2009. Spatial mapping of submerged cave systems by means of airborne electromagnetics: an emerging technology to support protection of endangered karst aquifers. *Near Surface Geophysics, Special Issue on Hydrogeophysics – Methods and Processes*, 7(5-6), 613-627.
- Supper, R., Schiller, A., Jochum, B., Ottowitz, D. 2010. *Geophysikalische Messungen in Tulum (Mexiko) – 2010, Österreichische Akademie der Wissenschaften*, online-ISBN: 978-37001-6971-0, doi:10.1553/mab-geophys-tulum-2010.
- Vuilleumier, C., A. Borghi, P. Renard, D. Ottowitz, A. Schiller, R. Supper and F. Cornaton, 2013. A method for the stochastic modeling of karstic systems accounting for geophysical data: an example of application in the region of Tulum, Yucatan Peninsula (Mexico). *Hydrogeology Journal* 21(3): 529-544.